Samy M. El-Behery
Faculty of Engineering,
Menoufiya University,
Shebin El-Kom, Egypt
e-mail: s_elbehery@yahoo.com

Mofreh H. Hamed
Faculty of Engineering,
Kafrelsheikh University,
Kafrelsheikh, Egypt
e-mail: mofrehhh@yahoo.com

K. A. Ibrahim
e-mail: kamalabd56@hotmail.com

M. A. El-Kadi
e-mail: mohamedelkady@yahoo.com

Faculty of Engineering,
Menoufiya University,
Shebin El-Kom, Egypt

CFD Evaluation of Solid Particles Erosion in Curved Ducts

This paper investigates numerically the erosion phenomenon that occurs in 90 deg and 180 deg curved ducts. The erosion prediction model comprises from three stages: flow modeling, particle tracking, and erosion calculations. The proposed three stages of the present model are tested and validated. Comparisons between predicted penetration rate and published experimental data show a good agreement. The effects of bend orientation, inlet gas velocity, bend dimensions, loading ratio, and particle size on the penetration rate are also simulated. In addition, based on many predictions of erosion rate results, new CFD based correlations are developed for the maximum penetration rate and its location. These correlations can be used to predict the bend lifetime for particular operating conditions. [DOI: 10.1115/1.4001968]

Keywords: pneumatic conveying, CFD, bend, gas-solid, erosion

1 Introduction

The erosion damage of the outer wall of the bends governed by many factors affects each other. The erosion of bends conveying gas-solid mixture was investigated by many researchers [1–14]. Earlier experimental studies were carried out by Bikbiaev et al. [1,2]. They found that the erosion rate increases as the inlet gas velocity and curvature ratio increase. Edwards et al. [3] developed CFD-based erosion prediction procedure and investigated the erosion in the 90 deg bend and plugged-tee. They found that the erosion in plugged-tee is less than that occurring in bends. Fan et al. [4] performed numerical and experimental investigation on ribbed bend and they concluded that the erosion was reduced due to the presence of ribs. Hanson et al. [5] developed a model to predict the life of pneumatic conveyor bend with an accuracy of ±65%. Wang and Shirazi [6] developed a CFD based correlation to predict the erosion ratio between long radius elbow and standard elbow. They found that the erosion rate decreases as the bend radius increases, while the predictions of Li [7] are counteracted with that of Wang and Shirazi [6]. Also, Burnett et al. [8] investigated the wear that occurs at long radius bends. The particle diameter is an important parameter in the erosion rate; McLaury [9] suggested that the erosion rate increases with increasing particle diameter up to 100 μm. Salama [10] suggested a particle diameter of 400 μm as a limiting value. He concluded also that the erosion rate is not affected by the particle size after this limit. In the investigation given by Niu and Tsao [11], the erosion rate increases as the particle diameter increases. This behavior was demonstrated for both 90 deg and 180 deg curved ducts. On the other hand, Mills and Mason [12], Kuki et al. [13], and Suzuki et al. [14] indicated that the erosion rate decreases with increasing particle diameter. From the previous discussion, it is clear that the erosion phenomenon is more complex and there are many parameters affecting each other. Also the U-bend meets very little interest. Therefore, the aim of present study is to investigate the erosion behavior in both the 90 deg and 180 deg curved ducts in order to evaluate the ability of the existing computational methods to simulate such flows

2 Governing Equations

The numerical calculations are performed using the Eulerian approach for gas-phase, taking into account the mutual effects of the solids on the air, and the Lagrangian approach for dispersed-phase, considering that all the particles have been introduced in the flow with approximately the same bulk velocity of the fluid. In a previous study [15], comparisons between four turbulence models, namely, standard k-ε model of Launder and Spalding [16], RNG based k-ε model of Eghlimi et al. [17], low-Re k-ε model of Launder and Sharma [18], and high-Re k-ε model of Kim and Chen [19] were performed. These comparisons showed that the RNG based k-ε turbulence model of Eghlimi et al. [17] predicts the flow within the bend better than other models. Therefore, the RNG based k-ε is recommended in the present study. Movements of particles are simulated by accounting for all important forces. The coupling effect of solid particles on the gas-phase is described through modifications of gas-phase equations. This is achieved by introducing the void fraction, which is defined as the volume of a phase divided by the volume of the two phases, and momentum exchange source term in the gas-phase equations. The gas-phase is considered as a continuous phase, and the solid phase is accounted for as a dispersed-phase. Some simplifying assumptions are made to provide a reasonable solution for engineering objectives.

2.1 Model Assumptions

1. The flow model is for a two-dimensional bend; therefore, the influence of spanwise velocity on the particle motion is not included.
2. The particles are spherical in the particle tracking procedure. However, the erosion ratio model in the present study is based on the experimental data for sand particles (the erosion ratio is defined as the ratio between mass loss of the target material and the mass of particles impinging on the target material).
3. The effect of interparticle collisions is ignored since the inertial effects prevail.

Table 1 Constants values of the RNG based k-ε model

C_μ	χ	η_o	B_k	B_ε
0.0845	0.015	4.38	0.09	0.4

4. The duct wall was assumed to be smooth and the particles are rigid during particle wall collisions.
5. The effects of turbulent flow velocity fluctuations on the particles are not considered. This assumption reduces the applicability of the model to geometries that redirect the flow such as elbows. The effects of turbulent fluctuations on the particle motion cannot be ignored such as flow with particles in straight pipes [6].
6. The ratio between particle density and gas density is very high so the effects of added mass force and pressure gradient force on the particle are neglected in the present study.

2.2 Gas Flow Modeling. The general form of elliptic differential equations governing two-dimensional, turbulent, steady, incompressible and isothermal two-phase flow through curved duct with upstream and downstream straight ducts is given as

$$\frac{1}{y^j}\frac{\partial}{\partial y}(\alpha\rho y^j v\Phi) + \frac{1}{y^j}\frac{\partial}{\partial \theta}(\alpha\rho u\Phi) = \frac{1}{y^j}\frac{\partial}{\partial y}\left(\alpha\Gamma_\Phi y^j\frac{\partial\Phi}{\partial y}\right)$$
$$+ \frac{1}{y^j}\frac{\partial}{\partial \theta}\left(\alpha\Gamma_\Phi\frac{\partial\Phi}{y^j\,\partial y}\right) + S_\Phi - S_S^\Phi$$
$$+ \rho g^\Phi \qquad (1)$$

where $j=1$, $y=r$ for curved duct, while for straight ducts $j=0$, $\theta=x$, and S^Φ and S_S^Φ are the source terms of gas and dispersed-phases, respectively, while the effective viscosity and the exchange coefficient, Γ_Φ, are summarized and reported in Ref. [16] for the dependent variable Φ. Constants of the used model are given in Table 1.

The RNG provides an analytically derived formula for the effective eddy viscosity that accounts for low-Reynolds number effects, as given in Ref. [17] as

$$\mu_{\text{eff}} = \mu\left[1 + \sqrt{\frac{C_\mu\rho}{\mu}\frac{k}{\sqrt{\varepsilon}}}\right]^2 \qquad (2)$$

The RNG k-ε model was derived using a rigorous statistical technique (renormalization group theory), which accounts for the effect of swirl on turbulence and provides an analytical formula for turbulent Prandtl numbers, σ_k and σ_ε, as follows:

$$\left|\frac{\lambda - 1.3939}{\lambda_o - 1.3939}\right|^{0.6321} + \left|\frac{\lambda + 2.3939}{\lambda_o + 2.3939}\right|^{0.3679} = \frac{\mu}{\mu_{\text{eff}}} \qquad (3)$$

where λ is the inverse Prandtl number (i.e., $\sigma_k = \sigma_\varepsilon = 1/\lambda$) with $\lambda_o = 1$.

The additional term in the dissipation rate equation (the rate of strain R) that significantly improves the accuracy for rapidly strain flow [17] is expressed as

$$R = \frac{C_\mu\eta^3(1 - \eta/\eta_o)}{1 + \chi\eta^3}\frac{\varepsilon^2}{k} \qquad (4)$$

where

$$S = \sqrt{G/\mu_t}, \quad \eta = S\frac{k}{\varepsilon} \qquad (5)$$

2.3 Particulate Phase Modeling. The solid phase is simulated using the Lagrangian approach. A few thousands of computational particles (i.e., parcels) were traced through the flowfield in each coupled iteration. After each given time step, the new position of the parcels and the new transitional and angular velocities are calculated from the equations of motion as in Ref. [20] through

$$\frac{dX_p}{dt} = U_p \qquad (6)$$

$$m_p\frac{dU_p}{dt} = F_D + F_{LS}F_{LR} + F_g \qquad (7)$$

$$I_p\frac{d\omega_p}{dt} = T \qquad (8)$$

$$T = \pi\mu D_p^3[0.5\nabla \times U - \omega_p] \qquad (9)$$

where X_p is the particle position vector, U, U_p are the gas and particle velocity vectors, ω_p is the particle angular velocity vector, T is the torque acting on the particle, $I_p = 0.1m_p D_p^2$ is the particle moment of inertia, m_p is the particle mass, F_D, F_{LS}, F_{LR}, and F_g are the components of the force arising from drag, shear lift, Magnus lift due to particle rotation, and gravity, respectively, and calculated as follows,

a. The drag force is calculated from

$$F_D = \frac{3}{4}\frac{\rho m_p}{\rho_p D_p}C_D(U - U_p)|U - U_p| \qquad (10)$$

where C_D is the drag coefficient and calculated as depicted in Ref. [21] as follows:

$$C_D = \frac{24}{\text{Re}_p}, \quad \text{Re}_p \le 1 = \frac{24}{\text{Re}_p^{0.646}}, \quad 1 < \text{Re}_p \le 400$$
$$= 0.5, \quad 400 < \text{Re}_p < 3 \times 10^5 \qquad (11)$$

where $\text{Re}_p = \rho D_p|U - U_p|/\mu$ is the particle Reynolds number.

b. The slip shear lift force is based on the analytical result of Saffman [22] and extended for higher Reynolds numbers according to Mei [23]:

$$F_{SL} = 1.615D_p\mu\,\text{Re}_S^{0.5}\,C_{SL}[(U - U_p) \times \omega_f] \qquad (12)$$

where $\omega_f = 0.5(\nabla \times U)$ is the fluid rotation, $\text{Re}_S = \rho D_p^2|\omega_f|/\mu$ is the particle Reynolds number of the shear flow, and $C_{SL} = F_{sl}/F_{sl,\text{Saff}}$ represents the ratio of the extended lift force to the Saffman force and given by

$$C_{SL} = (1 - 0.3314\gamma^{0.5})e^{-\text{Re}_p/10} + 0.3314\gamma^{0.5}$$
$$= 0.0524(\gamma\,\text{Re}_p)^{0.5} \qquad (13)$$

where γ is the correction function proposed by Mei [23] and is defined by the ratio between Re_s and Re_p as

$$\gamma = \frac{\text{Re}_s}{0.5\,\text{Re}_p} \qquad (14)$$

c. The Magnus lift due to particle rotation is expressed as in Ref. [20] by

$$F_{LM} = \frac{1}{2}\rho V_r^2\frac{\pi D_p^2}{4}C_{LM}\frac{\omega_r \times V_r}{|\omega_r||V_r|} \qquad (15)$$

where the quantities $V_r = U - U_p$ and $\omega_r = \omega_f - \omega_p$ are the relative linear and angular velocities between the local fluid and the particle, respectively. The Magnus lift coefficient may be expressed as in Ref. [20] by

$$C_{LM} = \frac{D_p|\omega_r|}{|V_r|}, \quad \text{Re}_p \le 1 = \frac{D_p|\omega_r|}{|V_r|} \quad (0.178$$
$$+ 0.822\,\text{Re}_p^{-0.522}), \quad 1 < \text{Re}_p < 1000 \qquad (16)$$

d. The gravity force is given by

$$F_G = m_p g \left(\frac{\rho}{\rho_p} - 1 \right) \quad (17)$$

For the calculation of particle motion, the equations of particle motion are integrated using fourth order Runge–Kutta method. To achieve this, the local values for the linear and angular velocity components, the liquid viscosity, turbulent kinetic energy and its dissipation rate at the location of the particle are required. These local values at the particle center are linearly interpolated from values at the closest grid nodes of the fluid finite-difference scheme enclosing the particle.

2.4 Coupling Between the Two Phases. The particles occupy the computational cell and reduce the gas volume fraction. They also exert interaction forces on the surrounding gas-phase. Thus, the two phases are coupled through the gas volume fraction and through the total source term, S_s^Φ, that accounts for the momentum exchange between solid particles and the gas-phase (two-way coupling).

The void fraction for dispersed-phase, β, and for gas-phase, α, are calculated using trajectory method, as given in Ref. [24] as

$$\beta = \sum_{traj} \frac{n_k \Delta t_k V_p}{V_C}, \quad \alpha = 1 - \beta \quad (18)$$

Here, n_k is the number of actual particles in the computational particle (parcel) k, per unit time, Δt_k, is the cell crossing time, V_P is the volume of the particle, V_c is the volume of computational cell, and Σ_{traj} means summing over all trajectories passing through the computational cell. It was assumed that each parcel contains several particles with the same properties and the number of actual particles in each parcel is obtained by dividing the total number of flowing particles by the number of simulated parcels. The source term of dispersed-phase in the gas momentum equation is calculated as in Ref. [20] by

$$S_S^{u,v} = \frac{\beta \rho_p}{m_p n} \sum_{k=1}^{n} (F_{D_k} + F_{LR_k} + F_{LS_k}) \quad (19)$$

where n is the number of trajectories passing through the computational cell. In addition, the effect of particulate phase on the turbulent structure can be written as reported in Ref. [17] for k and ε equations, respectively, as follows:

$$S_S^k = 2k \left[\frac{\rho_p}{\tau_p} \right] \left[1 - \exp \left(-B_k \frac{\tau_p}{\tau_l} \right) \right] \quad (20)$$

$$S_S^\varepsilon = 2\varepsilon \left[\frac{\rho_p}{\tau_p} \right] \left[1 - \exp \left(-B_\varepsilon \frac{\tau_p}{\tau_l} \right) \right] \quad (21)$$

where $\tau_l = k/\varepsilon$ and τ_p is the particle relaxation time.

3 Erosion Model

Earlier studies on the erosion of metals due to the solid particles impact was carried out by Finnie [25] and Tabakoof et al. [26]. They found that the erosion rate is mainly affected by the angle and velocity of impact. Recently Meng and Ludema [27] presented a comprehensive review of twenty two erosion models. More recently, the researchers at the Erosion/Corrosion Research Center (E/CRC) at the University of Tulsa [3,6,9] performed a series of numerical and experimental investigations on the erosion of metal surface by solid particles impact. According to Ref. [9], the erosion rate in the present study is given by

$$ER = A F_s W_{p1}^n F(\alpha_1) \quad (22)$$

where ER is the erosion rate (kg/kg), which is defined as the ratio between mass lost of target material to the mass of sand hitting it, and A and n are empirical constants. While $F(\alpha_1)$ is the function of impact angle and material being eroded and defined as

Table 2 Empirical constants for erosion model

	Material	
	Carbon steel	Aluminum
A	$4.223 BH^{-0.59}$	6.467×10^{-10}
α_o	15 deg	10 deg
a	-38.4	-34.79
b	22.7	12.3
ϖ	1	5.205
Ψ	3.147	0.147
Ω	0.3609	-0.745
χ	2.532	1
n	1.73	1.73

$$F(\alpha_1) = \begin{cases} a\alpha_1 + b\alpha_1, & \alpha_1 \le \alpha_o \\ \Psi \cos^2 \alpha_1 \sin(\varpi \alpha_1) + \Omega \sin^2 \alpha_1 + \chi, & \alpha_1 > \alpha_o \end{cases} \quad (23)$$

The values of the empirical constants based on W_{p1} in m/s are given in Table 2. In this table, BH is the Brinell hardness for carbon steel. W_{p1} and α_1 are the impact velocity and impact angle, respectively, as shown in Fig. 1. The F_S coefficient accounts for sand sharpness, its value being given as 1, 0.53, and 0.2 for sharp, semirounded, and rounded grains, respectively.

4 Solution Procedure and Model Validations

A hybrid discretization scheme is used for the momentum, turbulent kinetic energy, and dissipation rate equations of the gas-phase, while the equations of particle motion are integrated using the fourth order Runge–Kutta method. The mathematical model using the Eulerian–Lagrangian approach, as well as wall erosion submodel, was implemented in a FORTRAN program in which the
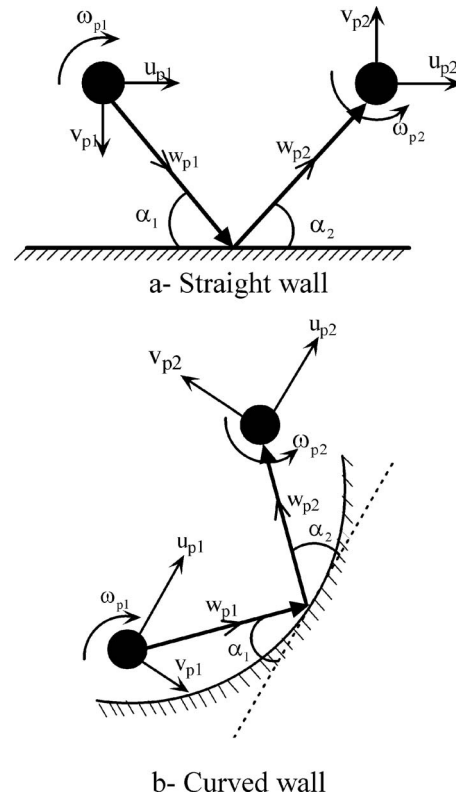

a- Straight wall

b- Curved wall

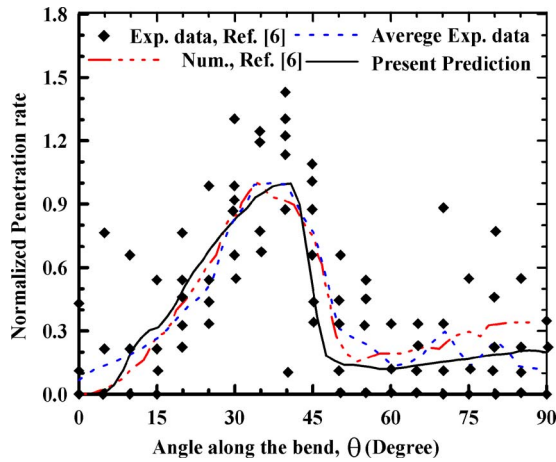**Fig. 1 Definition of velocities and angles before impact and after rebound**

Fig. 2 Comparison between predicted penetration rate and experimental data reported in Ref. [6], (U_o=50 m/s and Mr=2.8)
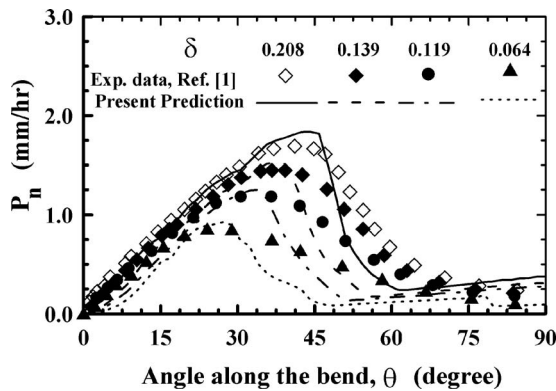

Fig. 3 Comparison between predicted penetration rate and experimental data of Ref. [1], (U_o=50 m/s and Mr=2.8)

equations of motion are repetitively solved for each representative particle. The continuous phase flow is obtained using the SIMPLE approach described by Patankar [28]. The motion of each parcel is then followed in a Lagrangian frame using the forces generated by fluid motion and gravity. The effect of particles on the local flowfield must then be modeled and fed back into the flowfield for the next iteration of gas calculations. The procedure is repeated until the maximum error in the axial gas velocity between the two successive coupled iterations is less than 0.5% of the inlet mean velocity.

The selection of the space grid will influence the solution obtained. The grid selection represents a compromise between the accuracy and computer time. At the beginning of each run case, the computer program performs the calculation for gas-phase only for different grid sizes. The axial gas velocity at bend exit was compared; if the difference in axial gas velocity between fine grid and coarse one is less than 0.5% of the mean gas velocity, the coarse grid was chosen. In the early stages of this investigation, the effect of grid on the penetration rate profile was also studied. It was found that the grid that gives independent solution of the flowfield was sufficient to give independent penetration rate profile. The number of simulated parcels and the time step were selected to give independent penetration rate profile. To reach this condition, several simulations are performed using different time steps and deferent number of parcels for each condition.

The prediction procedure of the proposed model comprises three stages, namely, flow modeling, particle tracking, and erosion calculations. Comprehensive validations of the first two stages were made by the present authors [15]. Therefore, the validation of the third stage is presented herein.

In the present study, the penetration rate, P_n (m/kg), is evaluated by dividing the erosion rate in kg/kg by the local cell face area and by the density of pipe wall material. If the penetration rate in m/kg is multiplied by the solid mass flow rate in kg/s, then the penetration rate in m/s will be obtained.

Figure 2 shows a comparison between the present predicted results, the numerical data of Wang and Shirazi [6], and the measured data of penetration rates reported in Ref. [6]. This figure shows that the model overpredicts the maximum penetration rates. While Fig. 3 shows a comparison between the present predicted and measured penetration rates of Bikbiaev et al. [1] at different curvature ratios. This figure shows also that the model overpredicts the maximum penetration rates for all curvature ratios. This is because the concentration of the sand in the experiments was very high (Mr=2.8). Since, in high concentration rate situation, interactions between particles reduce particle inertia and hence reduce erosion rate. Therefore, the major contribution to the dis-
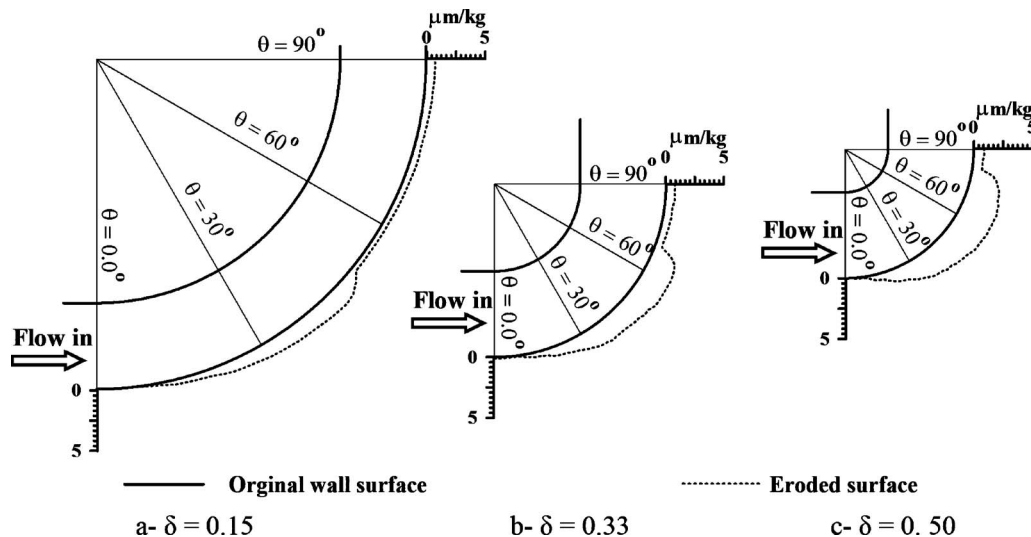

Fig. 4 Effect of curvature ratio on the penetration rate distribution along the outer wall of 90 deg bends
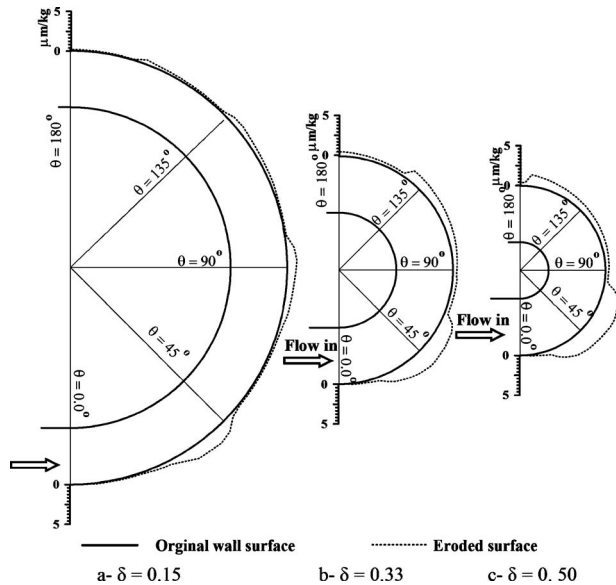
Fig. 5 Effect of curvature ratio on the penetration rate distribution along the outer wall of 180 deg bends

Fig. 7 Effect of inlet gas velocity on the penetration rate distribution along the outer wall of 90 deg and 180 deg bends

crepancy between predicted values and the data of Bikbiaev et al. [1] may be due to the interaction between sand particles, which is neglected in the present model.

5 Results and Discussion

In this section, numerical predictions of sand erosion phenomenon in 90 deg and 180 deg bends are presented. Also, the effects of different parameters on the penetration rate are studied. The effects of different operating parameters on the penetration rate distribution along the outer wall of 90 deg and 180 deg bends, as well as the impact location, are given in Figs. 4–14 with respect to the base case, which is given in Table 3. It can be seen from the figures that, in general, all parameters have a similar effect on the penetration rate in 90 deg and 180 deg. The results obtained for 90 deg bends indicate one peak for the penetration rate while that of 180 deg bends contain more than one peak. This is due to the fact that the length of 180 deg bend is greater than that of 90 deg bend. Figures 4–6 indicate that as the curvature ratio increases, the penetration rate increases. This may be due to the fact that, in long radius bend, the particles impact over a large area and therefore cause less penetration. These figures indicate also that as the curvature ratio decreases, the maximum penetration occurs at smaller bend angle. This can be explained as the curvature ratio decreases, the first impact location occurs at a small bend angle, as shown in Fig. 6. Figure 5 indicates also that the penetration rate of 180 deg bend for the smaller curvature ratio ($\delta=0.15$) has more peaks than the other curvature ratio. This is due to the fact that as the curvature ratio decreases, the bend length increases and the impact and rebound angles decrease; as a result, the particles in longer bend experienced multiple collisions with the outer wall.
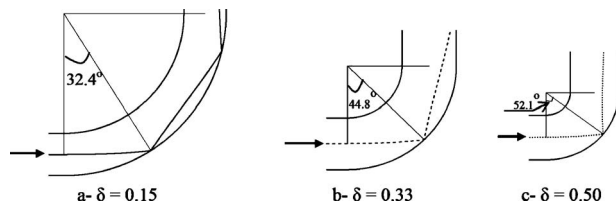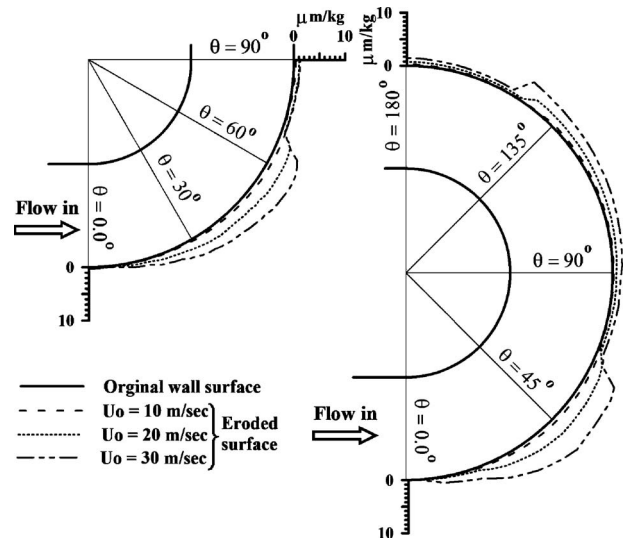
The effect of inlet gas velocity on penetration rate is shown in Fig. 7 for 90 deg and 180 deg bends. This figure indicates that as the inlet gas velocity increases, the penetration rate increases. This is due to the fact that as the inlet gas velocity increases, the impact
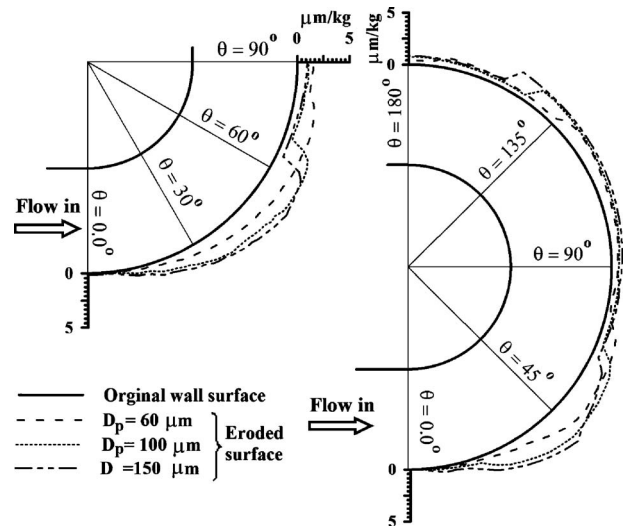

Fig. 8 Effect of particle diameter on the penetration rate distribution along the outer wall of 90 deg and 180 deg bends
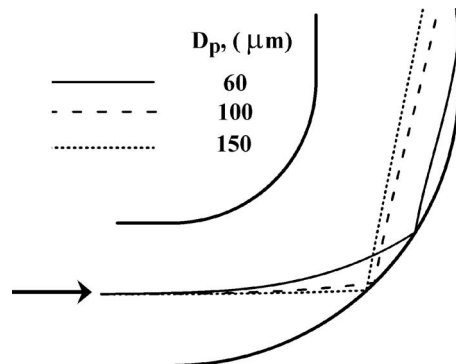

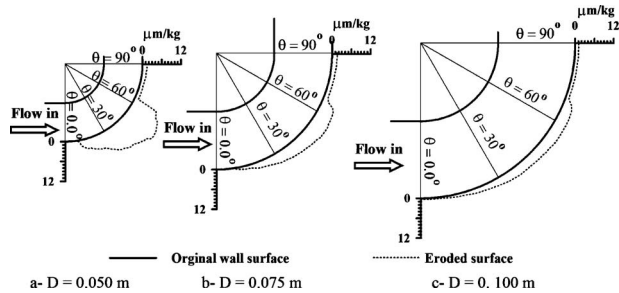Fig. 9 Effect of particle diameter on the impact location for a particle located at pipe center

Fig. 6 Predicted impact locations in different 90 deg bends for a particle located at pipe center
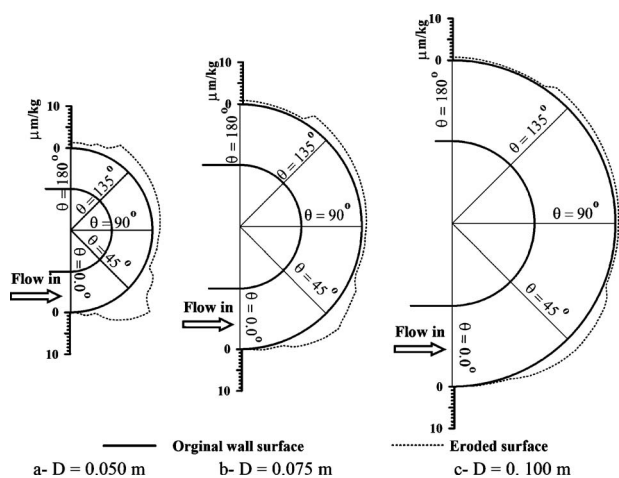
Fig. 10 Effect of pipe diameter on the penetration rate distribution along the outer wall of 90 deg bends
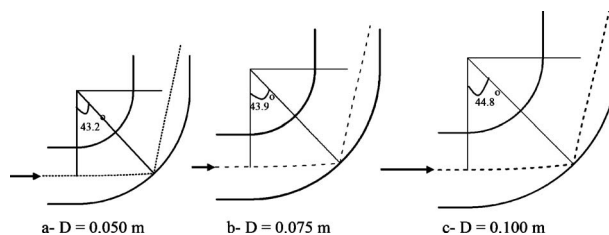

Fig. 12 Effect of pipe diameter on the impact locations for a particle located at pipe center

Fig. 11 Effect of pipe diameter on the penetration rate distribution along the outer wall of 180 deg bend
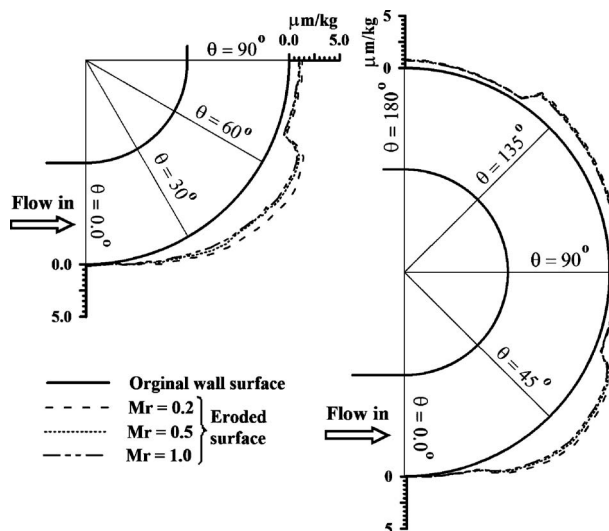

Fig. 13 Effect of mass loading ratio on the penetration rate distribution along the outer wall of 90 deg and 180 deg bends

velocity, which is taken directly in the erosion model, increases. It also indicates also that an increase in the inlet gas velocity gives slightly earlier maximum penetration. This is due to the fact that as the inlet gas velocity increases, the particles impact the outer wall of the bend at small bend angle.

The effect of particle diameter on the penetration rate is also studied by changing the particle diameter relative to the base case. Figure 8 shows the effect of particle diameter on the penetration rate in 90 deg and 180 deg bends. This figure indicates that the

Table 3 Condition of the base case for penetration rate calculations

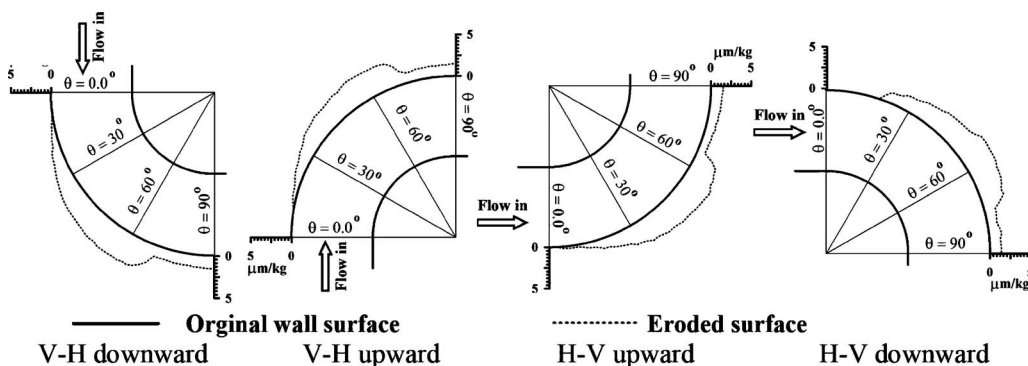| D_p (μm)	D (m)	ρ_p (kg/m^3)	Mr (kg/kg)	U_o (m/s)	δ
100	0.10	2650	0.5	20	0.33

Fig. 14 Effect of bend orientation on the penetration rate distribution along the outer wall of 90° bend
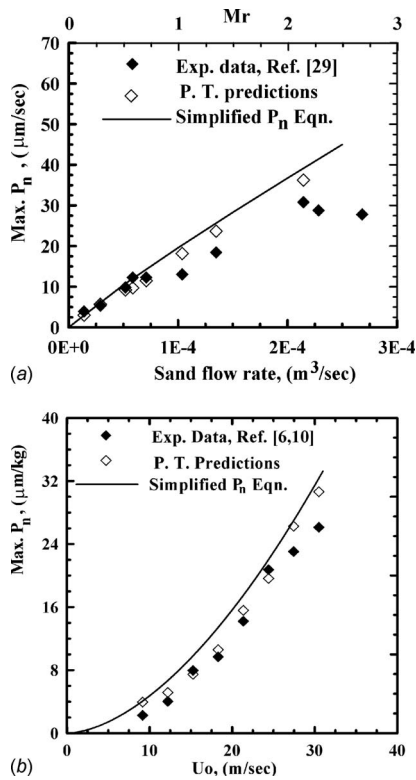
(a)

(b)

Fig. 15 Comparisons between particle tracking predictions (P. T.), simplified maximum P_n equation (Eq. (24)), and published data of Refs. [6,10,29]. (a) Effect of sand flow rate (or mass loading ratio) on the maximum penetration rate. (b) Effect of inlet gas velocity on the maximum penetration rate.

Fig. 16 Comparison between calculated P_n using simplified maximum P_n equation, (Eq. (24)), and published measured data

penetration rate increases as the particle diameter increases. This may be due to the fact that as the particle diameter increases, its inertia increases and the impact angle increases. It also indicates also that as the particle diameter increases, the maximum penetration occurs at a lower bend angle. This is due to the fact that the larger particle flows in straighter path from the proceeding pipe than that of smaller one and impacts the outer wall at lower bend angles, as shown in Fig. 9.

Figures 10 and 11 present the effect of pipe diameter on the penetration rate for the 90 deg and 180 deg bends. These figures indicate that the penetration rate increases as the pipe diameter decreases. This can be explained that as the pipe diameter increases, the particles are impacted over a large area causing less penetration. The results also indicate that as the pipe diameter increases, the maximum penetration occurs at high bend angles. This is due to the fact that as the pipe diameter increases, the
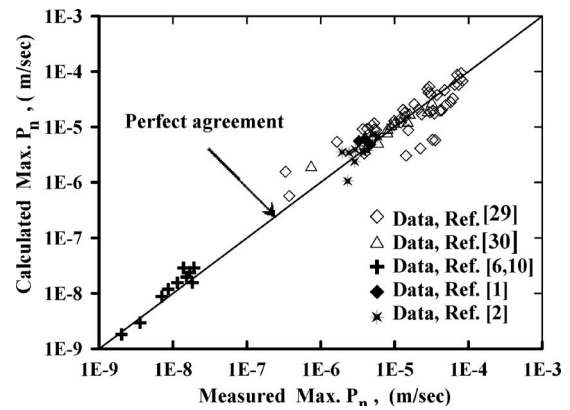
particles have relatively large time to respond to the change in flow direction and impact the outer wall at higher bend angles, as shown in Fig. 12.

The effect of mass loading ratio on the penetration rate in the 90 deg and 180 deg bends is shown in Fig. 13. This figure indicates that as the mass loading ratio increases, the penetration rate decreases. This can be explained that as the mass loading ratio increases, the momentum lost from particles to gas-phase increases and the particles impact with the outer wall at low inertia. The effect of bend orientation on the penetration rate is given in Fig. 14. This figure indicates that the penetration rate is less affected by the bend orientation. For the sake of simplicity, one can consider that the penetration rate of all bends is approximately the same as that of H–H bend.

The erosion prediction requires a prediction of particle impact speed and angle; also the impact location and impact intensity are needed. Therefore, this process could be very complex and time-consuming because trajectories of thousands of particles within the flowfield must be determined before the erosion rate in a bend can be estimated. Given the complexity of tracking solid particles in the flowfield within the bend and the need to track thousands of particles within the carrier gas, estimating penetration rate based on empirical relation appears to be a formidable task for many design engineers who may not necessarily be familiar with CFD and particle tracking in turbulent flows. Thus, the comprehensive flow models, particle tracking models, and erosion prediction methods developed to date are not practical design tools for a quick estimation of erosion rate in pipe bends. Therefore, in the present work, based on many CFD predictions of erosion rate and on the curve fitting of maximum penetration rate results, new CFD based correlations are developed and recommended to be used as an approximate engineering calculations to account for the effect of different flow and geometrical parameters on the maximum penetration rate in 90 deg bends.

$$P_n|_{max}(\mu m/kg) = \begin{cases} \dfrac{6.74 \times 10^{-4} F_s \cdot BH^{-0.59} \cdot D_p^{0.595} \cdot U_o^{1.61}}{D^{1.7} \cdot Mr^{0.1} \cdot e^{0.068/\delta}}, & D_p \le D_{pcr} \\[3mm] \dfrac{0.012 F_s \cdot BH^{-0.59} \cdot U_o^{1.63}}{D^{1.66} \cdot Mr^{0.0924} \cdot e^{0.069/\delta}}, & D_p > D_{pcr} \end{cases} \tag{24}$$

where

$$D_{pcr} = 126 \frac{U_o^{0.034} \cdot D^{0.068} \cdot Mr^{0.013}}{e^{1.71 \times 10^{-3}/\delta}} \tag{25}$$

In the above equations D_{pcr} is defined as the particle size in micrometers at which the penetration is not affected by the particle diameter. This behavior, from the authors' point of view, is

due to the fact that as the particle diameter increases, the particle inertia and impact angle increase, which leads to an increase in the penetration rate. On the other hand, the number of particles within the flow field decreases for constant mass loading ratio, which leads to a decrease in the penetration rate. Thus, at a certain particle diameter, D_{pcr}, depending on the flow and geometrical parameters, the two effects vanish each other. For a wide range of operating conditions, the critical particle, D_{pcr}, is found to vary between 100 μm and 150 μm.

To validate the proposed correlation, the maximum predicted penetration rate and the calculated one using the proposed simplified equation, Eq. (24), are compared with the experimental data of Bourgoyne [29] and data reported in Refs. [6,10], as shown in Fig. 15. It can be seen from Fig. 15(a) that the present correlation agrees well with the experimental data up to $Mr=1.0$; further increase in mass loading ratio, the correlation and particle tracking predictions overpredict the maximum penetration. This may be due to the fact that as the mass loading increases, the number of particles within the flowfield increases, which results in an increase in particle-particle collisions. As a result of particle collisions, the particle momentum decreases and hence the penetration rate decreases. Since the effect of particle-particle collision is not included in the present model, the maximum penetration rate at

high mass loading ratios is overpredicted. On the other hand, the correlation and particle tracking prediction agree well with the experimental data reported in Refs. [6,10], as shown in Fig. 15(b). Furthermore, the predictions by the present correlation and the available experimental data in the literature are compared, as shown in Fig. 16. This figure indicates an acceptable agreement between the present calculated maximum penetration rates and the measured ones [30].

Figure 17 presents comparisons between predicted maximum penetration rates by particle tracking and calculated ones by the CFD correlations, at different conditions. This figure indicates that, the present correlations agree well with the numerical predictions for a wide rang of operating and geometrical conditions.

The bend lifetime can be increased by coating the inside surface of the outer wall with a high-hardness alloy or applying a protective lining (such as alumina cement or middle manganese nodular cast iron). Another method to protect bends from erosion is ripped bend protection [4]. The first method leads to increase the cost of manufacturing, while the second one increases the pressure drop. However, this can be minimized by locating the position of major erosion zone. During the course of simulation, it was observed that the location of maximum penetration is greatly affected by the curvature ratio and particle size. Thus, larger particles flow in
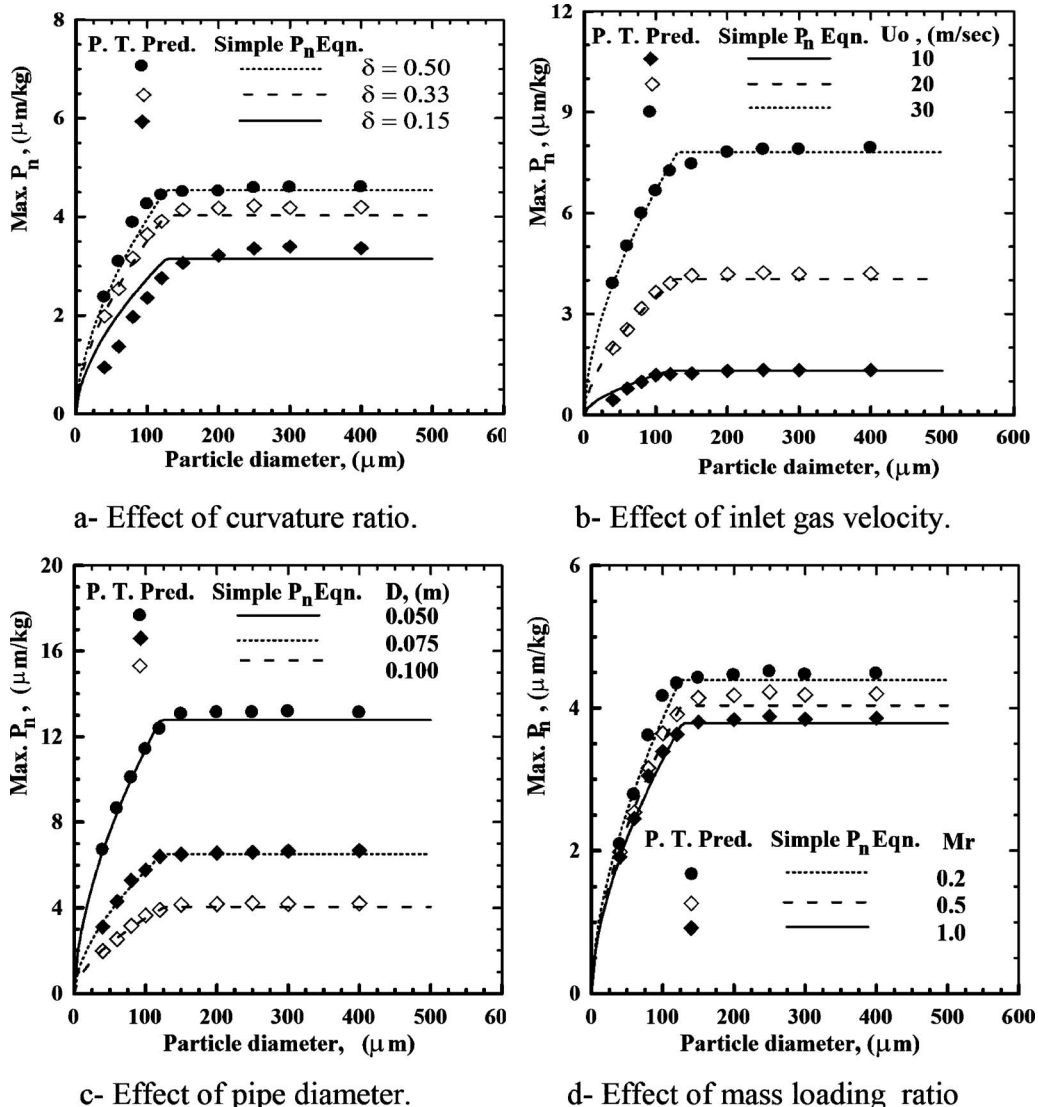

a- Effect of curvature ratio.

b- Effect of inlet gas velocity.

c- Effect of pipe diameter.

d- Effect of mass loading ratio

Fig. 17 Comparisons between the present particle tracking predictions (P. T.) and simplified maximum P_n equation (Eq. (24)) for 90 deg bend
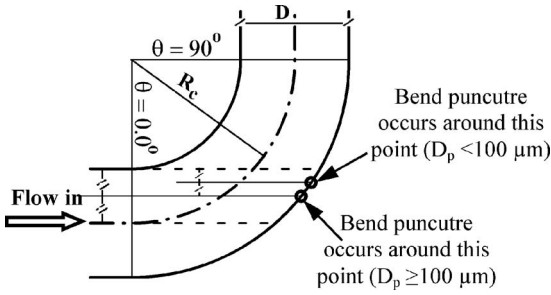
Fig. 18 A schematic representation of the location of bend puncture point

straighter lines causing bend puncture, approximately, at the mid-point between the extensions of preceding straight pipe inner wall and centerline, as shown in Fig. 18. On the other hand, the smaller particles are affected by the surrounding flow field (i.e., if the flow velocity is high, the bend puncture occurs at small bend angle, while for low conveying velocity, the puncture occurs at large bend angle). However, it was observed that the location of maximum penetration for small particles occurs around a point slightly downstream that of large particles, as shown in Fig. 18.

Based on the present predictions of the location of maximum penetration rate and on the bend geometry, Fig. 18, the following simple equation is developed to calculate the location of maximum penetration, θ_{max}, as a function of the bend curvature ratio, δ.

$$\theta_{max} = \begin{cases} \cos^{-1}\left(\dfrac{1-\delta/2}{1+\delta}\right) \pm \theta_{err}, & D_p \geq 100 \quad \mu m \\ \cos^{-1}\left(\dfrac{1-3\delta/4}{1+\delta}\right) \pm 2.5\,\theta_{err}, & D_p < 100 \quad \mu m \end{cases}$$

(26)

where

$$\theta_{err} = \cos^{-1}\left[\frac{1}{4(1+\delta)^2}(4 - \delta(1 - \sqrt{(\delta+2)(15\delta+40)}))\right] \quad (27)$$

In the above equation, θ_{err} is an error band that accounts for the change in the location of maximum penetration rate due to the change in operating conditions. The value of θ_{err} was found to be, approximately, 10% of the corresponding θ_{max}.

Figure 19 shows the comparison between the predicted location of maximum penetration rate using correlation (26), present numerical predictions, and published experimental and numerical data. It can be seen from the figure that the proposed equation agrees well the numerical and experimental data.

6 Conclusions

The RNG based k-ε turbulence model has been used to simulate the gas flow in the 90 deg and 180 deg bends, while Lagrangian particle tracking was used for particle motion calculations. The effects of particle rotation and lift forces were included in the model. The effect of solid phase on the gas-phase is also taken into account. The erosion calculations are based on the empirical model of McLaury [9]. The comparisons between the present prediction and the published experimental data show good agreement. The present result shows that the penetration rate increases as the curvature ratio, particle diameter, and inlet gas velocity increase, and as the mass loading ratio and pipe diameter decrease. Furthermore, the present study shows that the bend orientation and flow direction have no significant effect on the penetration rate. New correlations for predicting the maximum penetration rate and its location was developed and validated with available data.
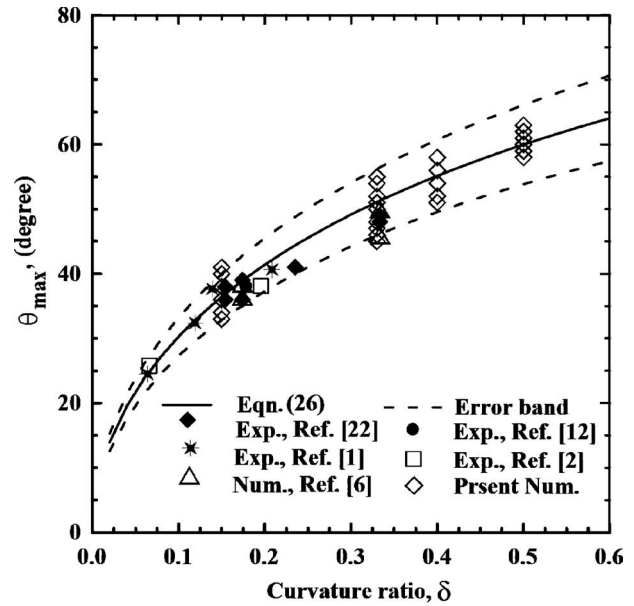
a- Dp ≥ 100μm
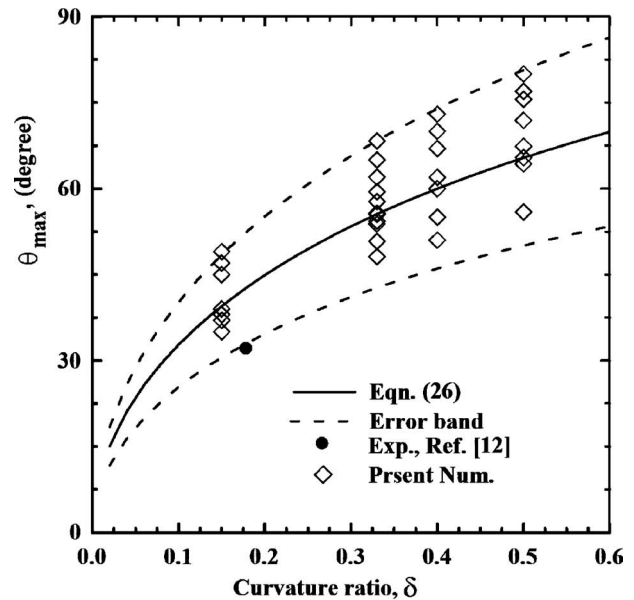
b- Dp < 100μm

Fig. 19 Comparisons between the predicted locations of maximum penetration rate, θ_{max}, using the proposed equation (Eq. (26)) and available data

Nomenclature

A, a = empirical constants in the erosion model
b = empirical constant in the erosion model
BH = Brinell hardness for carbon steel
D = diameter of bend, m
D_p = particle diameter, μm
ER = erosion rate, kg wall material/kg solid particles
F_s = sand sharpness factor
H-H = horizontal -to-horizontal
H-V = horizontal-to-vertical
k = turbulent kinetic energy, m^2/s^2
Mr = mass loading ratio, $(\mathring{m}_P/\mathring{m}_g)$
n = empirical constant in the erosion model

P_n = penetration rate, μm/kg
R_C = mean bend radius of curvature, m
t = time, s
u_p = mean axial particle velocity, m/s
v_p = mean radial particle velocity, m/s
$V\text{-}H$ = vertical-to-horizontal
U_o = mean-bulk longitudinal velocity, m/s
W_{p1} = particle velocity before impact, m/s

Greek Symbols

δ = curvature ratio $(D/2R_c)$
ε = turbulent kinetic energy dissipation rate, m^2/s^3
ϖ, Ψ = constants in the erosion model
μ = viscosity, kg/m s
$\Omega, \lambda,$ = constants in the erosion model
θ = axial coordinate along the bend, deg
ρ = density, kg/m^3
α_1 = impact angle, deg
α_2 = rebound angle, deg
ω_p = particle angular velocity, rad/s

Subscripts

1 = before impact
2 = after rebound
p = particle
w = wall

References

[1] Bikbaev, F. A., Maksimenko, M. I., Berezin, V. L., Krasnov, V. L., and Zhilinskii, I. B., 1972, "Wear on Branches in Pneumatic Conveying Ducting," Chem. Petrol. Eng., **8**, pp. 465–466.

[2] Bikbaev, K. A., Krasnov, V. I., Maksimenko, M. I., Berezin, V. L., Zhilinskii, I. B., and Otroshko, N. T., 1973, "Main Factors Affecting Gas Abrasive Wear of Elbows in Pneumatic Conveying Pipes," Chem. Petrol. Eng., **9**, pp. 73–75.

[3] Edwards, J., McLaury, B. S., and Shirazi, S. A., 2001, "Modelling Solid Particle Erosion in Elbows and Plugged Tees," ASME J. Energy Resour. Technol., **123**, pp. 277–284.

[4] Fan, j., Yao, J., Zhang, X., and Cen, K., 2001, "Experimental and Numerical Investigation of a New Method for Protecting Bends From Erosion in Gas-Particle Flows," Wear, **251**, pp. 853–860.

[5] Hanson, R., Allsopp, D., Deng, T., Smith, D., Bradley, M. S. A., Hutchings, I. M., and Patel, M. K., 2002, "A Model to Predict the Life of Pneumatic Conveyor," Proc. Inst. Mech. Eng. Part E J. Process Mech. Eng., **216**, pp. 143–149.

[6] Wang, J., and Shirazi, S. A., 2003, "A CFD Based Correlation for Erosion Factor for Long-Radius Elbows and Bends," ASME J. Energy Resour. Technol., **125**, pp. 26–34.

[7] Li, X., 1996, "Computational Simulation of Turbulent Single Phase and Multi-Phase Flow," Ph.D. thesis, Clarkson University, New York.

[8] Burnett, A. J., Pittman, A. N., and Bradley, M. S. A., 1998, "Observations on and the Modelling of Erosive Wear of a Long-Radius Pneumatic Conveyor Bend," Proc. Inst. Mech. Eng., Part J: J. Eng. Tribol., **212**, pp. 369–379.

[9] McLaury, B. S., 1996 "Predicting Solid Particle Erosion Resulting From Turbulent Fluctuation in Oilfield Geometries," Ph.D. thesis, University of Tulsa, Tulsa, OK.

[10] Salama, M. M., 2000, "An Alternative to API 14E Erosional Velocity Limits for Sand-Laden Fluids," ASME J. Energy Resour. Technol., **122**, pp. 71–77.

[11] Niu, Y.-Y., and Tsao, J.-C., 2002, "Numerical Evaluation of Erosion in Curved Duct," Numer. Heat Transfer, Part A, **41**, pp. 341–356.

[12] Mills, D., and Mason, J. S., 1977, "Particle Size Effects in Bend Erosion," Wear, **44**, pp. 311–328.

[13] Kuki, J., Toda, K., and Yamamoto, M., 2003, "Development of Numerical Code to Predict Three-Dimensional Sand Erosion Phenomena," ASME Paper No. FEDSM2003-45017.

[14] Suzuki, M., Toda, K., and Yamamoto, M., 2003, "Numerical Investigation on Wavy Streak Formation Due to Sand Erosion," ASME Paper No. FEDSM2005-77074.

[15] El-Behery, S. M., Hamed, M. H., El-Kadi, M. A., and Ibrahim, K. A., 2009, "CFD Prediction of Air-Solid Flow in 180° Curved Duct," Powder Technol., **191**, pp. 130–142.

[16] Launder, B. E., and Spalding, D. P., 1974, "The Numerical Computation of Turbulent Flows," Comput. Methods Appl. Mech. Eng., **3**, pp. 269–289.

[17] Eghlimi, A., Kouzoubov, A., and Fletcher, C. A. J., 1997, " A New RNG-Based Two-Equation Model for Predicting Turbulent Gas-Particle Flows," Proceedings of the First International Conference on CFD in Mineral & Metal Processing and Power Generation Industries, Melbourne, Australia.

[18] Launder, B. E., and Sharma, B. I., 1974, "Application of the Energy-Dissipation Model of Turbulence to the Calculation of Flow Near a Spinning Disc," Lett. Heat Mass Transfer, **1**, pp. 131–137.

[19] Chen, Y.S., Kim, S.W., 1987, "Computation of Turbulent Flows Using an Extended k-ε Turbulence Clouser Model," NASA Report No. CR-179204.

[20] Lun, C. K. K., and Liu, H. S., 1997, "Numerical Simulation of Dilute Turbulent Gas-Solid Flows in Horizontal Channels," Int. J. Multiphase Flow, **23**, pp. 575–605.

[21] Kladas, D. D., and Deorgiou, D. P., 1993, "A Relative Examination of CD-Re Relationships Used in Particle Trajectory Calculations," ASME J. Fluids Eng., **115**, pp. 162–165.

[22] Saffman, P. G., 1965, "The Lift on a Small Sphere in a Slow Shear Flow," J. Fluid Mech., **22**(02), pp. 385–400.

[23] Mei, R., 1992, "An Approximate Expression for the Shear Lift Force on a Spherical Particle at Finite Reynolds Number," Int. J. Multiphase Flow, **18**, pp. 145–147.

[24] Crowe, C., Sommerfeld, M., and Tsuji, Y., 1998, *Multiphase Flow With Droplets and Particles*, CRC, Boca Raton, FL.

[25] Finnie, I., 1972, "Some Observation on the Erosion of Ductile Materials," Wear, **19**, pp. 81–90.

[26] Tabakoff, W., Kotwal, R., and Hamed, A., 1979, "Erosion Study of Different Materials Affected by Coal Ash Particles," Wear, **52**, pp. 161–173.

[27] Meng, H. C., and Ludema, K. C., 1995, "Wear Models and Predictive Equations: Their Form and Content," Wear, **181–183**, pp. 443–457.

[28] Patankar, S. V., 1983, *Numerical Heat Transfer and Fluid Flow*, McGraw-Hill, New York.

[29] Bourgoyne, A. T., 1989, "Experimental Study of Erosion in Diverter Systems Due to Sand Production," Proceedings of the SPE/IADC Drilling Conference, New Orleans, LA, pp. 807–816.

[30] Bourgoyne, A. T., Casariego, V., and Kelly, O. A., 1991, "Integrity of Diverter Systems Under Abrasive, Multi-Phase Flow," Summary Report, Petroleum Engineering Department, Louisiana State University, Baton Rouge, LA.